9950-687

DOE/JPL -956046-82/2
Distribution Category UC-63
Report #2

An EBIC Study of Dislocation Networks in Unprocessed and Unprocessed Web Silicon Ribbon

May 1982

JPL Contract No. 956046

by

F. Sporon Fieldler* and D. Ast

Materials Science and Engineering
Bard Hall, Cornell University
Ithaca, New York 14853

The JPL low-cost solar array project is sponsored by the U.S. Department of Energy and forms part of the Solar Photovoltaic Conversion Program to initiate a major effort toward the development of low-cost solar arrays. This work was performed for the Jet Propulsion Laboratory, California Institute of Technology by agreement between NASA and DOE.

* Permanent address: Hewlett-Packard Co, 1020 N.Circle Blvd, Corvallis, Or. 97330.

ABSTRACT

Experimental techniques for the preparation of EBIC samples of Web-dentritic silicon are described. Both as-grown and processed material were investigated. High density dislocation networks were found close to twin planes in the bulk of the material. The electrical activity of these networks is reduced in processed material for reasons which are not understood.

INTRODUCTION

Electron beam induced current (EBIC) microscopy is a useful tool for the microcharacterization of semiconductors. An EBIC micrograph is essentially a map of the spatial distribution of the minority carrier recombination centers in the semiconductor (1). In addition to providing an image of the electrical activity of the semiconductor on the scale of a μm or less, EBIC can also obtain quantitative information on the position of shallow trap levels in the band gap and the minority carrier diffusion lengths (2).

Ebic has been used in this study to investigate the defect structure of Web-dendritic silicon. The current interest in silicon web is due to its potential use as a substrate material for large scale solar cell arrays (3). The crystal growth method is described in detail by Dermatis and Faust (4) and is therefore only briefly discussed here. Figure 1 is an illustration of the growth process. Growth is initiated from a twinned <211> dendrite seed brought into contact with a supercooled melt. On withdrawing the seed, dendrites grow into the melt and a liquid film is drawn up between them which subsequently solidifies to form the web silicon ribbon. Web and dendrites have a <211> growth direction and a {111} surface orientation. The dendritic growth requires at least two twin planes which usually extend into the web (5). Other crystal imperfections such as dislocations are introduced into the web during growth. These defects may act as recombination centers for minority carriers, thereby reducing the efficiency of solar cells fabricated from the web.

Previous analysis of the defect structure of the web-dendritic silicon has been carried out by Cunningham et al. (6). A high voltage transmission electron microscope (1 MV) and a scanning microscope in the EBIC mode was used for this analysis. A high density dislocation network lying near the twin boundary region of the material was found. The network contained perfect and partial dislocations lying in <112> and <110> directions as well as a hexagonal network of partial dislocations confined to the twin plane. Their EBC study of the material, however, did not allow a detailed analysis of the electrical activity associated with the networks due to the problem of obtaining the twin plane close to the surface of the material, as required for EBIC imaging of the networks.

The present report describes an improved sample preparation method which allows one to image the dislocation networks in EBIC. Using this technique, samples of as grown material and material processed for solar cells were examined with EBIC at room temperature. A quantitative analysis of the trap levels in the energy gap associated with crystal defects was attempted by using temperature dependent EBIC (EBIC(T)).

EXPERIMENTAL

The EBIC micrographs of the material were obtained on an AMR 900 scanning electron microscope (S.E.M.) and a JEOL 733 S.E.M.. Both were operated with accelerating voltages in the range 11-21 kV and beam currents of ~1 nA. In the EBIC mode, the electron beam is used to generate electron hole pairs in the specimen. The EBIC image is formed by collecting the minority carriers at a Schottky barrier junction and displaying this signal on the S.E.M.'s CRT.

Enhanced recombination of minority carriers at defects reduces the collected current relative to defect-free regions and electrically active defects therefore appear dark on the EBIC display. Several excellent reviews are available on this technique (1,2,8,9).

The web-dendritic silicon was received from JPL in two forms: as-grown or processed. The as-grown material is 10 ohm-cm p-type (boron doped) and was supplied in the form of strips ~30x3x0.1 cm. The processed material arrived in the form of a 3x3x0.1 cm solar cell fabricated on the as-grown material. The solar cells have a diffused p-n junction on the front surface of the cell (Phosphorous CVD with subsequent drive-in diffusion) and a diffused aluminum ohmic back contact.

Upon receipt, the materials were cut up into ~1x1x0.1 cm pieces with a diamond-tipped pen. The pieces were mounted on a stainless steel polishing block with thermosetting wax. At this stage, it is important to ascertain that the pieces are resting very flat on the polishing block. A flat surface is necessary as the twin plane must lie within 5 microns of the surface for the defect structures to be imaged in EBIC. The most effective way of achieving this is to mount the sample as flat as possible on the polishing block. Since the sample is invariably tilted very slightly, one obtains a very shallow bevel. This geometry is depicted in Figure 2. The bevel angles achieved with this method are typically <1 degree. (Previous workers (6) raised one side of the sample with a support in order to get a bevelled sample. This technique, however, gives larger bevel angles and only a very narrow strip (<40 microns wide) of the twin plane networks lies therefore within reach of the electron beam.) The polishing is started with 600 grit Silicon Carbide (SiC) powder. The surface of the sample is inspected every

30 seconds until the twin planes can be seen cutting through the surface. At this stage, the polishing is continued with 800 grit SiC (30 secs) and 1000 grit SiC powder. The polishing step is completed by Syston polishing the sample until a mirror-smooth surface is obtained.

Immediately following polishing, the sample is moved from the polishing block and cleaned as follows:

1. Ultrasonic rinse in organic solvents:
    a. Tricholorethylene (1 min)
    b. Acetone (1 mir)
    c. Methanol (1 min)
    d. Rinse in deionized water
2. Inorganic Cleaning:
    a. Warm bath in 5:2:1 H_2O:H_2O_2:NH_4OH (15 mins, 80 C)
    b. Rinse in deionized water
3. Ionic cleaning
    a. Warm bath in 7:2:1, H_2O:H_2O_2:HCl (15 mins, 80 C)
    b. Rinse in deionized water

The cleaning is completed with a 60 sec. etch in $5H_2O$:1 HF in order to remove any native oxide present on the surface of the sample prior to evaporation. After the etch, the sample is immersed in isopropanol during transport to the evaporator.

A 500 Angstrom Aluminum later is e-beam evaporated onto the backside of the sample in a vacuum of $<10^{-6}$ Torr. The sample is then annealed at 535 C for 30 mins in a hydrogen atmosphere (10 mm Hg) to form an ohmic contact on the back surface of the sample. (Processed web material already contains an ohmic back contact so that this step is omitted. After the

evaporation, the back contact is painted with Lacomit to protect the aluminum. The sample is again etched in $5H_2O$:1 HF to remove any oxide that may have formed and a 200 Angstrom layer of aluminum is then evaporated onto the front surface of the sample through a 3x3 mm square metal grid. Schottky barriers are hereby formed on the surface of the sample. The sample preparation is completed by removing the Lacomit from the backside and by mounting the sample on an aluminum disk with carbon-conducting paint. Figure 3 is an S.E.M. photograph of a typical sample. The bright "finger" is a spring loaded copper contact to the Schottky barrier.

The EBIC signal from the Aluminum Schottky barrier is amplified with a Keithley 427 current amplifier, the output of which is fed into the video-amplifier of the S.E.M.

Room temperature EBIC micrographs were obtained on both the AMR and JEOL 733 scanning electron microscopes. In order to quantify the observed electrical activity, a temperature dependent EBIC experiment was initiated. Measurements of the EBIC current profile of a defect as a function of temperature yield information on the electronic level associated with the defect (11,12). Two limiting cases have been discussed in the literature: i) A temperature dependent cross-section, as the Fermi level passes through the defect level (12), and ii) changes in the effective lifetime of the minority carriers which spend more time in shallow traps as the temperature decreases (12). In the latter technique, the temperature dependent minority carrier diffusion length, L(T), must be extracted from EBIC measurements. The theory then predicts that $L^2 \cdot \sqrt{T}$, when plotted vs 1 kT, should yield straight lines of slope -E, where is energy level of the defect measured from the band edge.

Figure 4 is a diagram of the experimental layout for EBIC(T) on the AMR 900 S.E.M.. The temperature stage consists of a Joule-Thompson Cycle refrigerator capable of achieving temperatures between 77 and 300 K.

A manual scan mechanism allows one to slowly scan the electron beam across a particular defect and the resulting profil is plotted out on an external Houston 2000 X-Y plotter connected to the deflection and video circuits of the S.E.M..

In order to collect the EBIC current from the sample, a new EBIC contact was designed. Figure 5a is an illustration of the holder. Figure 5b is a top view of the holder and refrigerator in place on the microscope. Two contacts are available, enabling one to monitor the Czochralski reference sample as well as the test sample. The coiled tubes at the top of the photograph are the gas supply lines for the Joule-Thompson refrigerator.

A Faraday cup was installed in order to measure the current of the incident beam. Speciment current was measured with a digital Keithly electrometer.

Preliminary experiments showed that it was essential to reduce contamination of the sample during cold operation. A cold finger which is cooled to liquid nitrogen temperatures prior to cooling the sample was therefore fabricated and installed into the S.E.M.. Figure 6a is a schematic of the cold finger design. Figure 6b shows the cold finger in place on the microscope sample chamber wall. The cold finger tip is a semi-circular Copper disk located approximately 1/2 cm above the sample surface during operation.

Figure 7 is a photograph of the experimental layout for the temperature dependent EBIC. The cold finger and sample stage are visible under the electron optical column. Signal amplifiers are located in the right background

and the refrigerator's gas controller is seen in the back of the electron column.

RESULTS AND DISCUSSION

Room Temperature EBIC of Twin Boundary Networks

Examination of the surface of the as-grown web revealed that this sample contains at least 5 twin planes. Figure 8 is an optical micrograph of the surface of the sample. The 5 twins observed are numbered consecutively. Twin number 1 is the outermost twin with the others lying deeper in the foil. The curvature at the top of the micrograph is a polishing artefact due to the bevelled nature of the sample and the large white areas are the Aluminum Schottky diodes.

Figure 9 is an EBIC map from Twin 1 (T1) down to Twin 2 (T2) (left to right). The region on the left side of T1 contains a high density of dislocations. As the twin trace through the sample surface is crossed by the interrogating beam, the dislocation density appears to drop due to the fact that the electron beam is at this point probing a volume which is too far above T2 to be influenced by dislocations on that plane. At 11 kV, the electron beam gauge is ~3 microns so that any defects located on T2 will only be visible in the vicinity of intersection of T2 with the surface. The dislocation density therefore increases as T2 is approached. Note that the dislocation density on this twin plane is much lower than that found on T1. The sequence is repeated as the beam moves onto T3, etc.

In all specimens investigated so far, the outer twin planes had invariably a higher defect density than those in the interior. The finding suggests that most of the dislocation contained in the twin planes are introduced during

cool down by interactions of the twins with bulk dislocations.

The dislocation network found on Tl is of the greatest interest due to the high density of recombination centers present. Figure 10 shows a typical region of the dislocation network found on this plane. Several types of dislocations can be observed. The long straight dislocations lying along <110> directions are perfect dislocations with burgers vectors lying in the inclined {111} planes, partial dislocations with 1/6<112>burgers vectors confined to the twin planes, or Lomer-Cottrell dislocations. These dislocations are discussed by Cunningham et al. (6). The appropriate crystallographic directions are indicated in Figure 10. The other dislocations observed are seen in more detail in Figures 11 and 12, which are higher magnification micrographs of the area marked (A) in Figure 10.

In Figure 11, the curved dislocations lying in the strip bounded by the straight dislocations marked (A) and (B) are either partial dislocations or perfect 90 or 30 degree dislocations (6). Figure 12 is a map of the hexagonal dislocation network in Figure 11. The network is similar to one discussed by Cunningham et al. (6), who found that the network consists of Shockley partials with orientations close to screw. A particularly interesting feature is the three-fold symmetry in the EBIC contrast from the hexagonal network. This is apparent when one examines the region marked (A) in Figure 12. Going clockwise around one of the dislocation hexagons, one sees alternating strong and weak EBIC contrast at nodes in the hexagonal network.

The three-fold symmetry is a consequence of the fact that an intrinsic (DSC) dislocation in a twin boundary invariably introduces a step in the boundary plane. Thus 3 jogs must be present in a hexagonal node in a planar {111} twin boundary with a twist component. Goodhew et al. have discussed

the geometry of such networks in great detail. The observed contrast is therefore compatible with a model that assumes that jogs are sites of enhanced electrical activity. Enhanced contrast is also observed where the network interacts with the straight <110> dislocations, such as at the point marked (B) in Figure 12, but these interactions have not yet been analyzed.

The EBIC Micrographs obtained from the processed web material are very different in character and intensity from those obtained from the as-grown material. The bevel angle on this sample is larger than the one on the as-grown sample, making the area of interest somewhat smaller. Two twin planes are evident on this sample, their traces extending as shown on Figure 13. A large number of parallel curved dislocations with line directions of ~<121> are present on T2. Their regular spacing of ~10 microns indicates that they all have burgers vector of the same sign. Very few dislocations with [110] directions are visible.

An interesting dislocation interaction is observed along the <110> line marked (A) in Figure 13. The line directions of all the parallel dislocations change abruptly from ~<121> to <110> over a short distance and then changes back to <121>. EBIC lacks the necessary resolution to analyze the interaction. Transmission electron microscopy studies are planned to examine this effect at higher resolution.

Figure 14 is a higher magnification image of the hexagonal network which can be seen faintly on T1 in Figure 13. This network also has a different appearance from that in unprocessed Web. Contrast is weak and no signs of three-fold symmetry can be detected. A markedly different appearance is also evident in the dislocation marked (A) with a <110> line direction. Certain segments of this dislocation show little or no contrast. The different

electrical activity of these defects when compared with similar defects in as-grown material strongly suggest that high temperature processing in effect decreases the electrically activity of many line defects, either by core reconstruction or the absorption of point defects. Strunk (10) has shown that point defects are introduced in front of a drive-in diffusion, such as the one required to generate the P-N junction at the front of the solar cell. These point defects are highly mobile and could diffuse to deep lying bulk dislocation. Further experiments are required to decide which mechanism is operating.

Upon completion of the experimental arrangement for temperature dependent EBIC, an attempt at quantifying the electrical behavior of the dislocation networks previously discussed was initiated. Figure 15a is a plot taken from the Houston X-Y plotter of the EBIC current as the electron beam was scanned across the defect shown in Figure 15b along the line a-a. This figure shows the feasibility of quantifying the electrical activity by monitoring the EBIC profile as a function of temperature. Temperature dependent EBIC profiles, however, were not obtained due to failure of maintaining a good ohmic contact to the sample at low temperatures. As the temperature was lowered, charging of the sample became frequent, leading to spikes in the EBIC current. The back contact has to be improved before quantitative analysis of the dislocation networks found in web-dendritic silicon can be carried out.

CONCLUSION

The preparation and examination of web-dendritic silicon with EBIC microscopy is described. As-grown material as well as processed material were examined, and both contained high density dislocation networks close to twin

planes in the bulk of the material. Hexagonal twist boundary dislocation networks were found to lie on the outermost twin planes of each sample. Processed and unprocessed material showed different dislocation structures with the processed material having a lower dislocation density. The lower activity observed in the processed material indicates that the electrical activity of most structural defects is reduced during the high temperature processing steps such as the drive-in diffusion.

Implementation of temperature dependent EBIC on an AMR 900 microscope was initiated. A new EBIC contact and cold finger for the microscope were fabricated and installed. Temperature dependent EBIC measurement were hampered by the fact that the conventional diffused aluminum ohmic contacts did not operate properly at low temperatures. Improvement of the contacts is needed before an energy level analysis of the dislocation networks can be carried out.

References

1. Leamy, H.J., Kimmerling, L.C., Ferris, S.D. Scanning Electron Microscopy, Vol. 1. (1978).

2. Hanoka, J.I., Bell, R.O. Ann. Rev. Mater. Sci., 11:353-80 (1981).

3. C.S. Duncan et al., JPL Technical Report, Contract No. NAS 954654, #80/4 (1980).

4. Dermatis, S.N., Faust, J.W. IEEE Trans Communications Electronics, 65, 194. (1963).

5. Seidensticker, R.G., J. Crystal Growth, 39, 17 (1977).

6. Cunningham, B., Strunk, H., Ast, D.G. JPL Report #320134, Cornell University. J. Electro. Chem. Soc. 129, 901 (1982).

7. Carter, C.B., Foell, H. Materials Science Center Report, No. 4280, Cornell University, July 1980.

8. Davidson, S.M., Journal of Miscroscopy, 111, 177 (1977).

9. Holt, D.B., Quantitative Scanning Electron Microscopy, Academic Press, New York, p. 182 (1976).

10. Goesele, U., Strunk, H. Applied Physics, 20, 265 (1979; Strunk, H., Goesele, U., and Kolbesen, B.O., J. Microscopy, 118, 35 (1980).

11. Hanoka, J.I., Bell, R.O., Bathey, B.R. (To be published in Symposium on Electrical and Optical Properties of Polycrystalline or Impure Semiconductors. (1980) E.C.S., Princeton, NJ).

12. Kimmerling, L.C., Leamy, H.Y., and Patel, Y.R., Applied Physics Lett., 30, 217 (1977).

Figure Captions

Figure 1: Schematic depiction of Web growth. Seed button, bounding dendrites and crystallographic orientation of the ribbon are indicated.

Figure 2: Illustration of sample geometry required for EBIC investigation of dislocation networks in Web silicon ribbon

Figure 3: S.E.M. photograph of Web sample. Squares are Schottky diodes. Bright "finger" is Copper contact.

Figure 4: Experimental layout for EBIC(T).

Figure 5: a. EBIC sample contact for EBIC(T).
b. Photograph of contact in place on microscope stage

Figure 6: a. Cold finger design for EBIC(T).
b. Cold finger in place on microscope

Figure 7: Photograph of modified AMR 900 microscope used for EBIC(T)

Figure 8: Optical micrograph of as-grown Web silicon ribbon.

Figure 9: EBIC map from twin plane T1 to twin plane T3 on as-grown material.

Figure 10: Dislocation network on twin plane T1.

Figure 11: Higher magnification micrograph of twin plane T1 network.

Figure 12: Hexagonal twist boundary network on twin plane T1 in as-grown material.

Figure 13: EBIC map of dislocation network in processed Web silicon ribbon.

Figure 14: Hexagonal network in processed Web silicon ribbon.

Figure 15: a. EBIC profile recorded on external X-Y plotter attached to modified AMR.
b. EBIC Image of defect recorded in 15a.

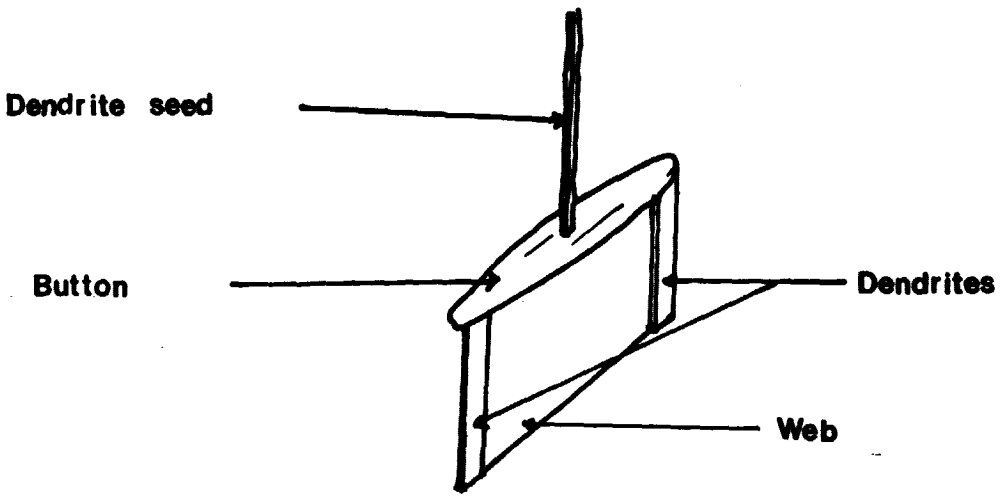

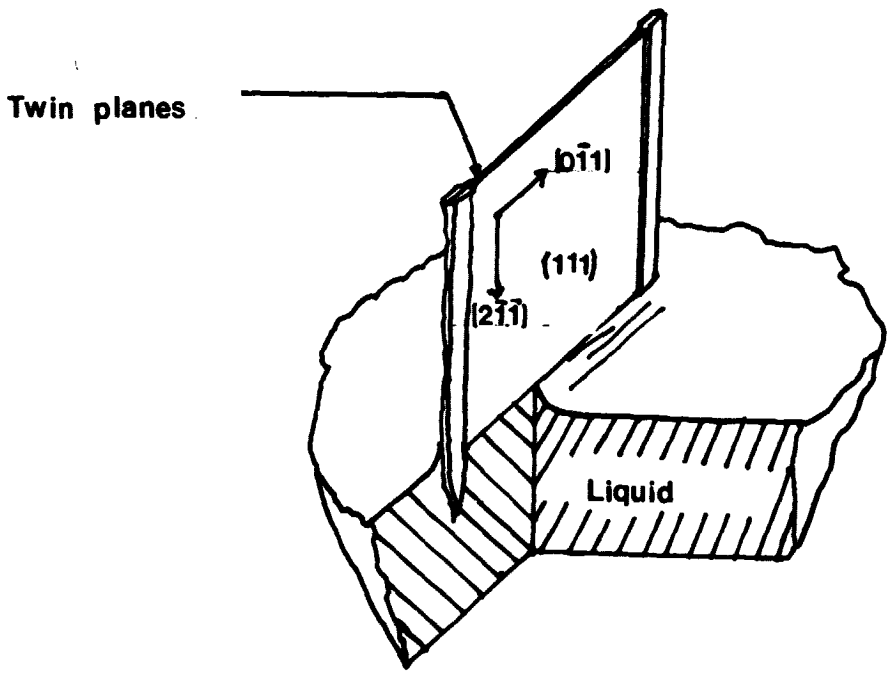

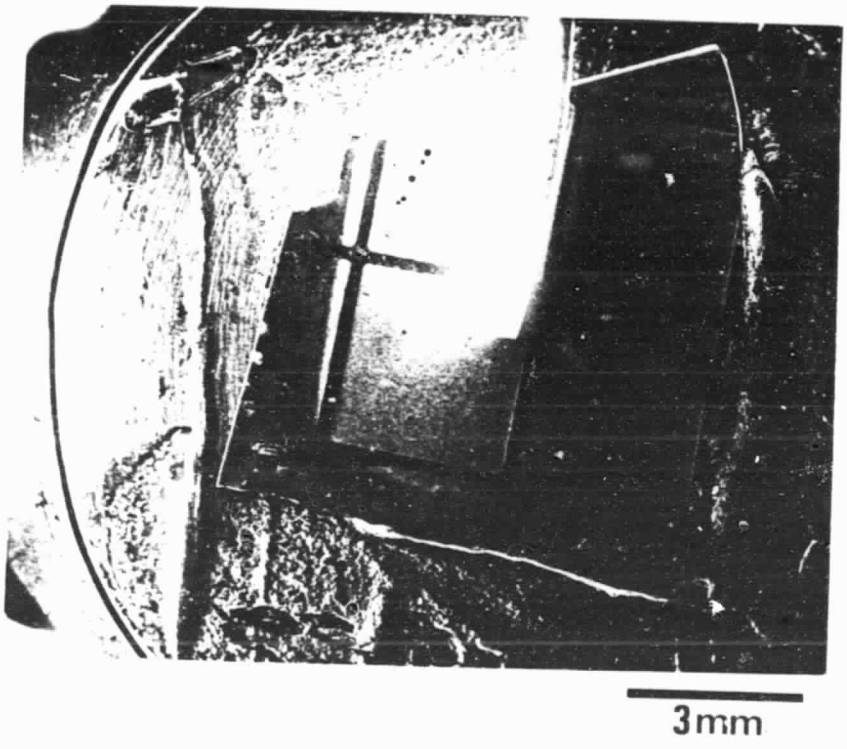

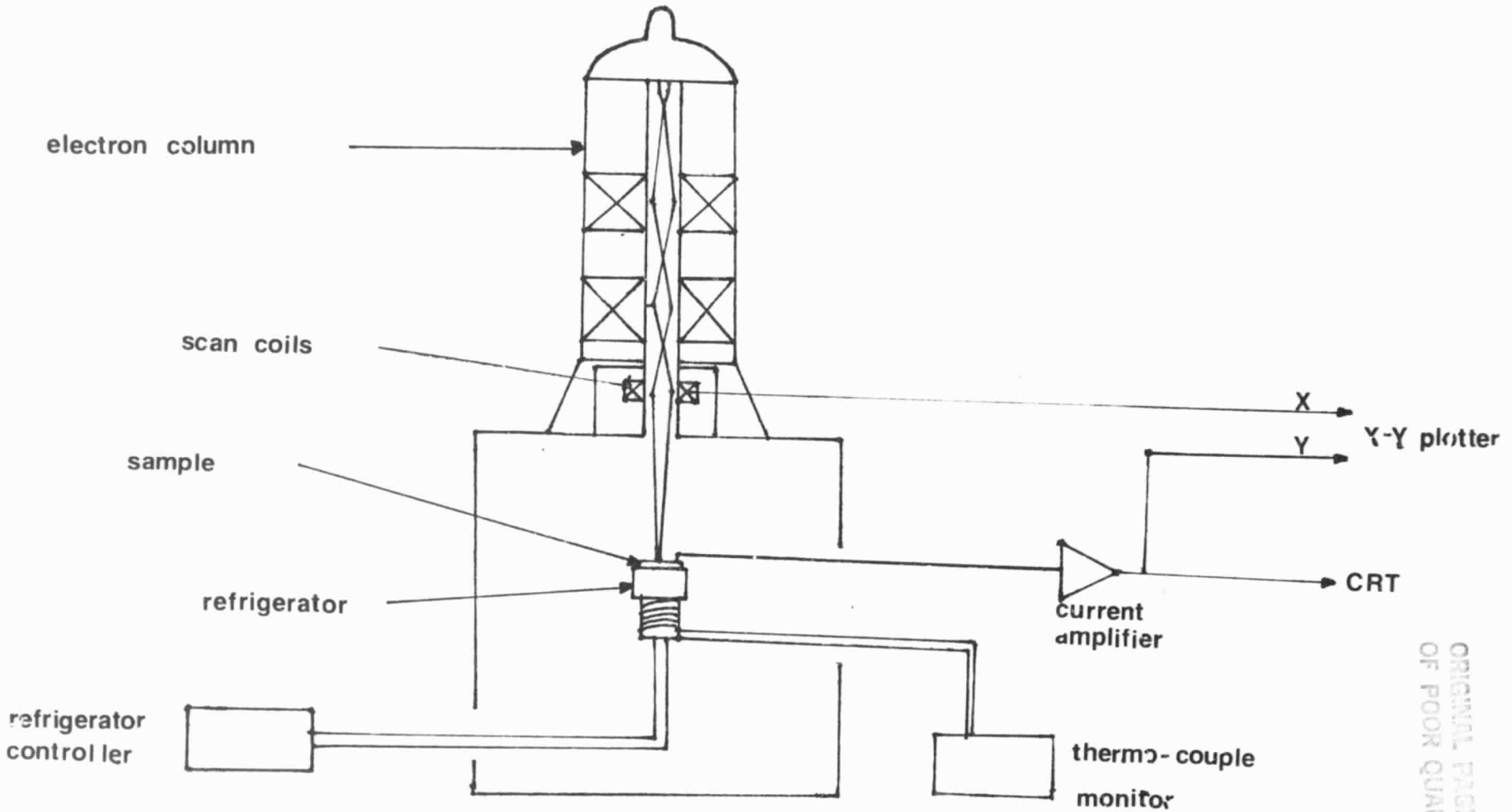

Experimental Lay-out for EBIC(T)

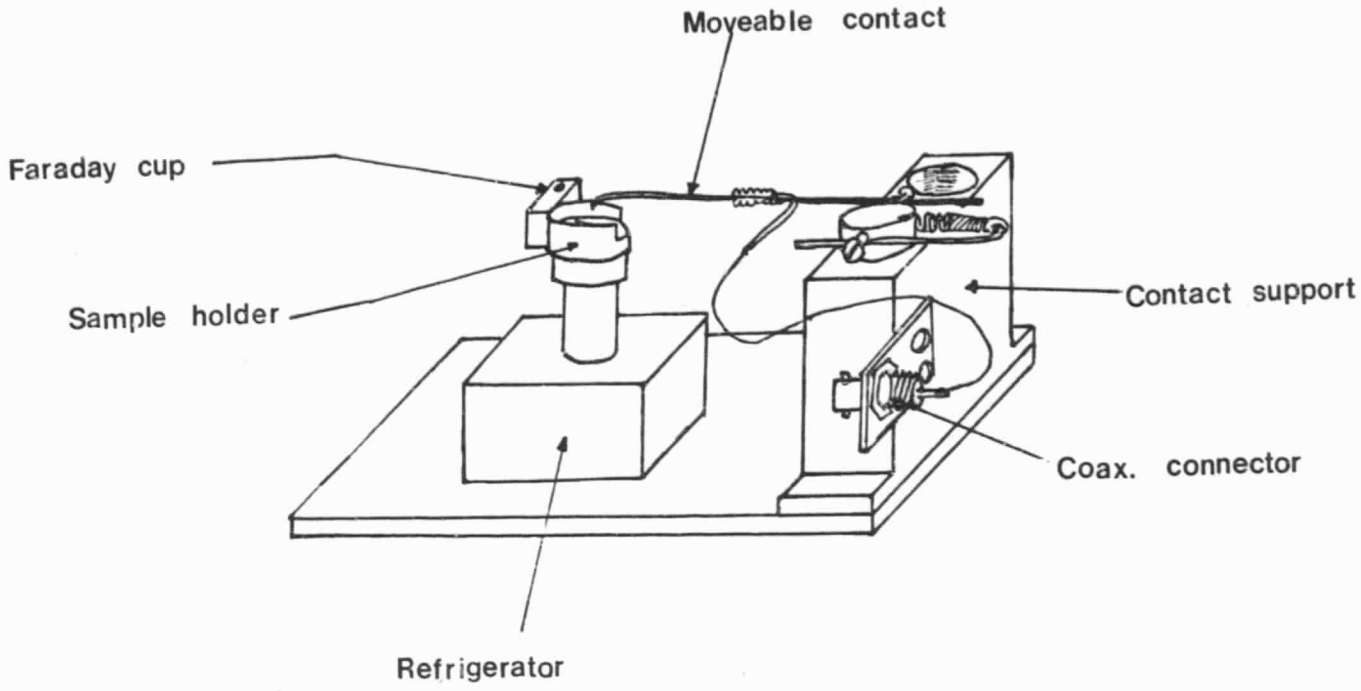

[A]

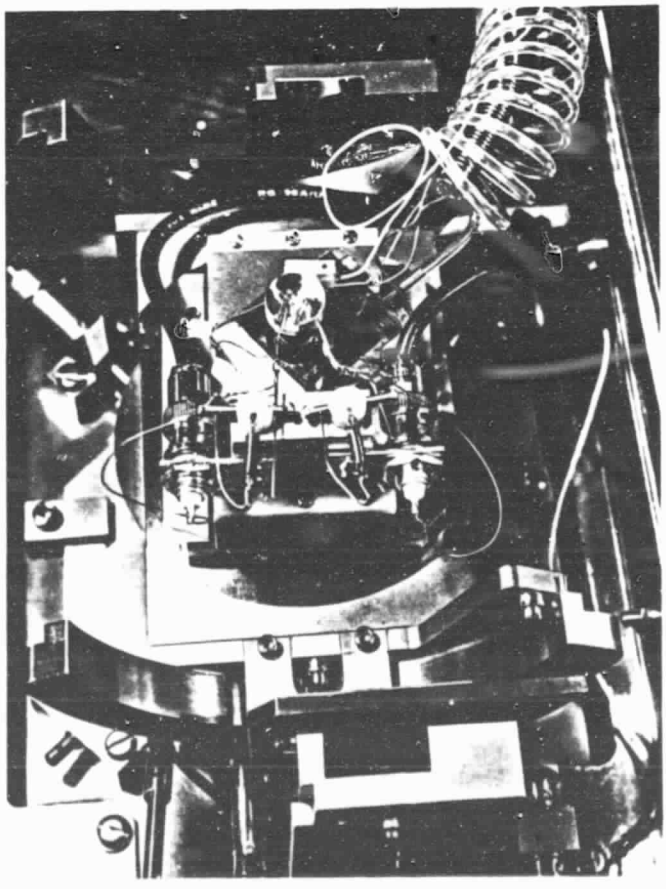

[B]

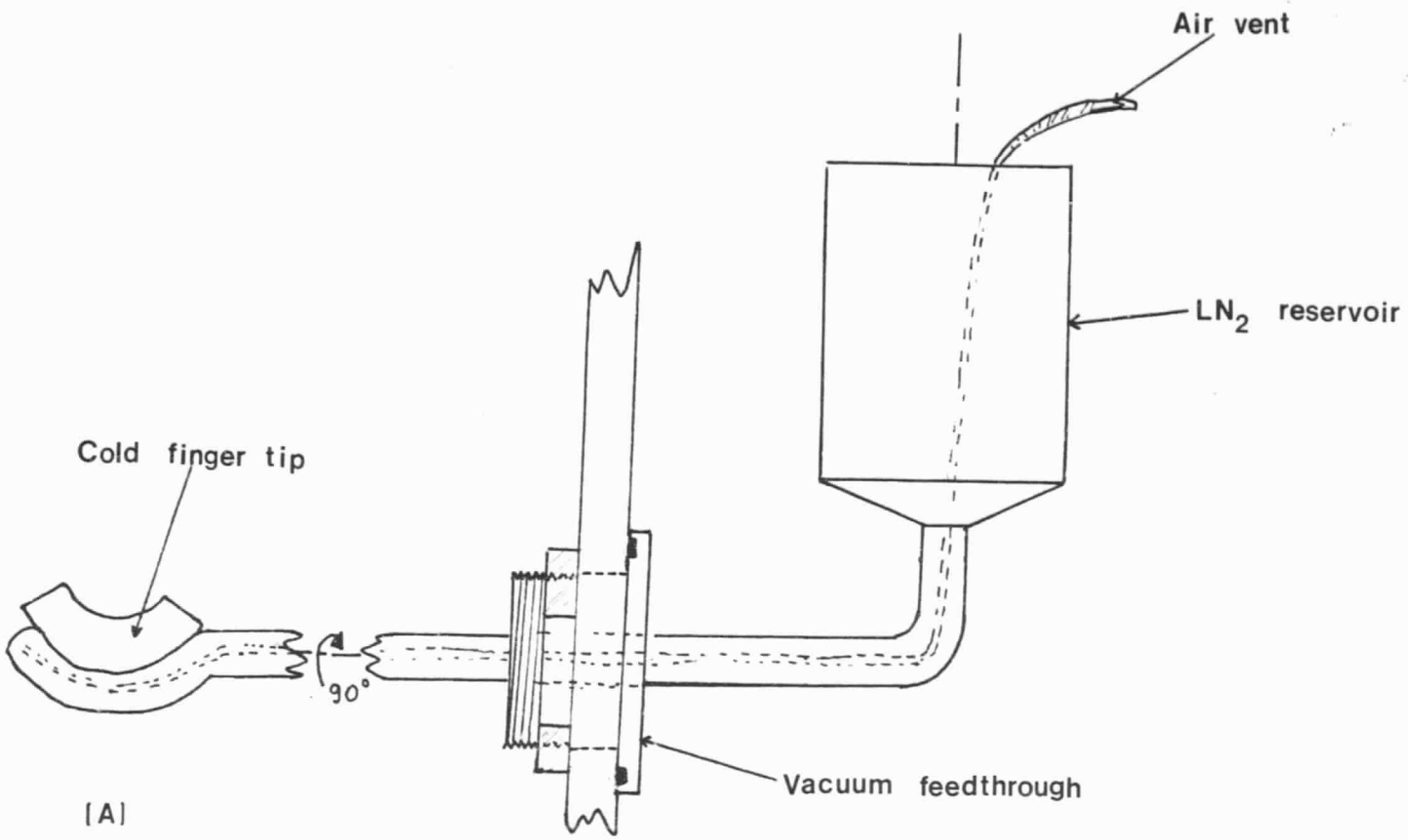

[A]

[B]

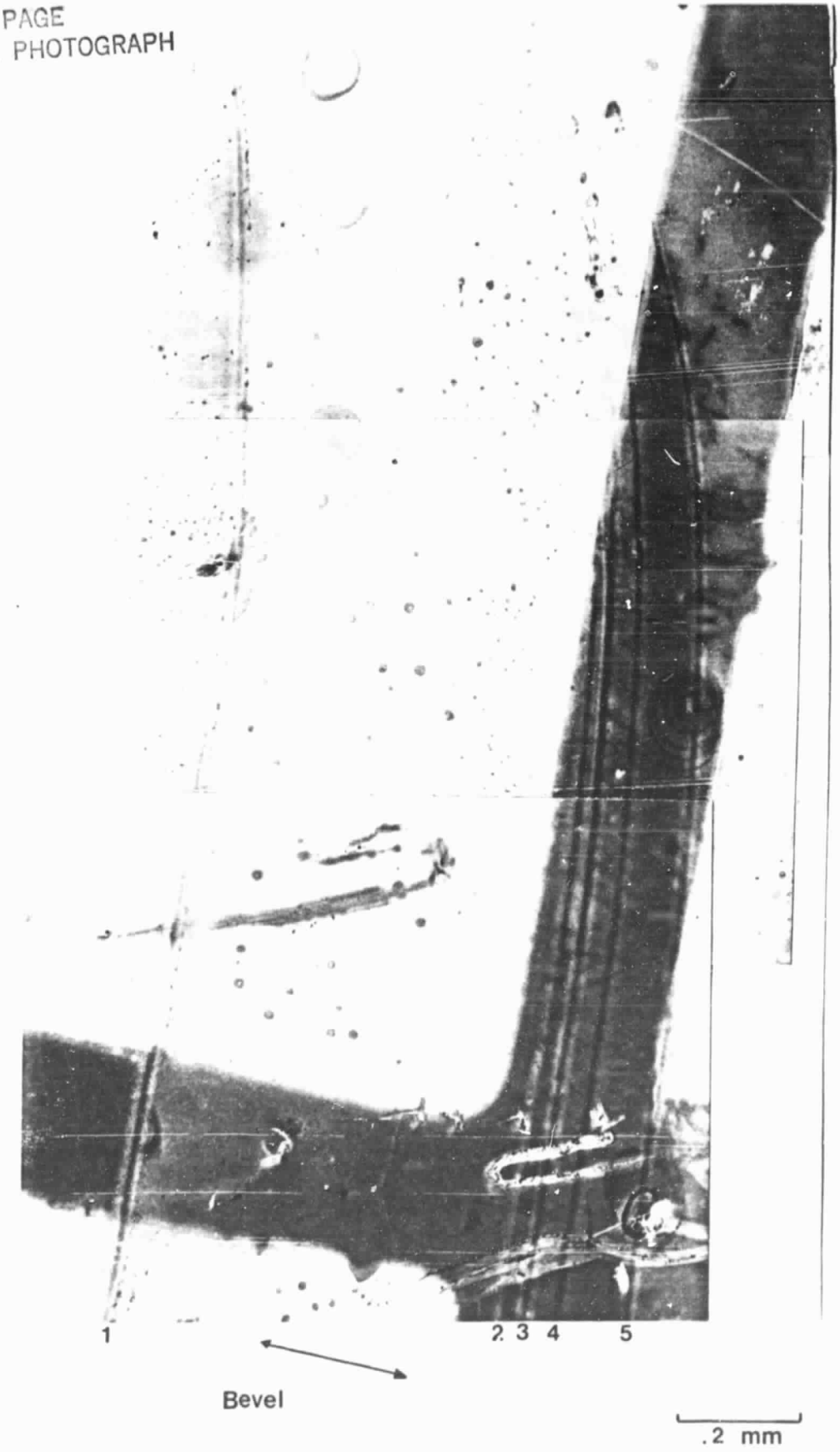

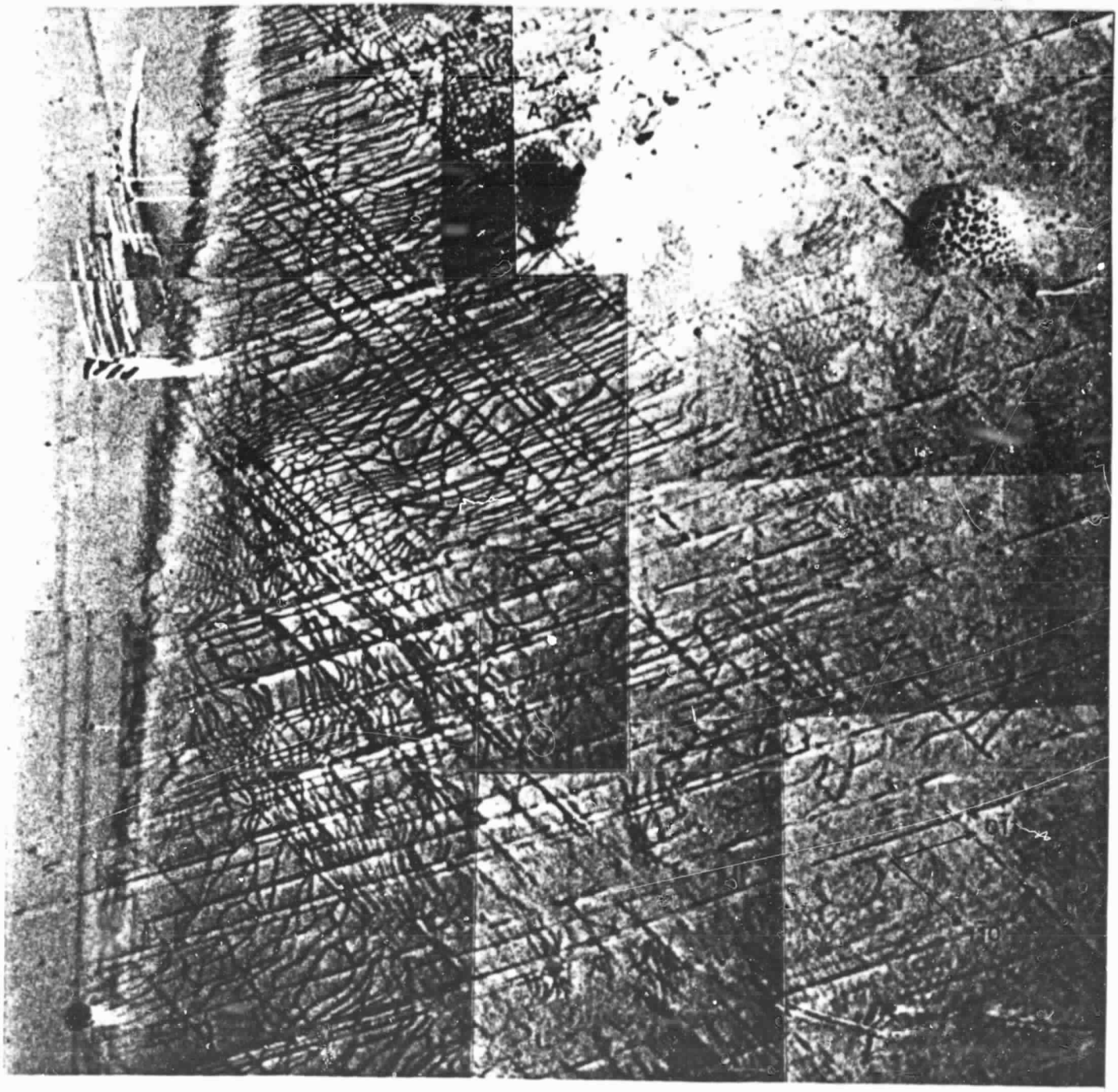

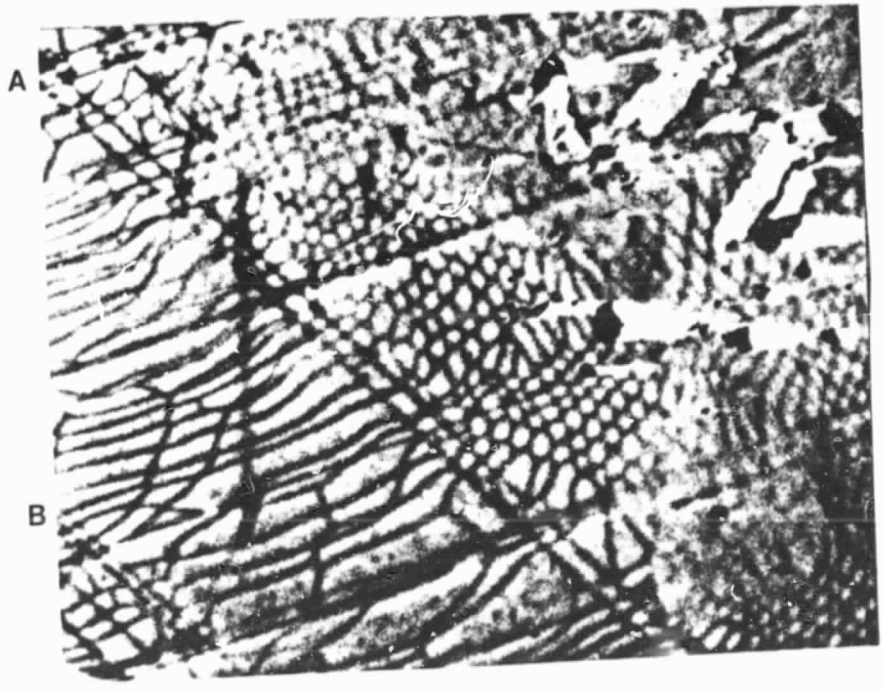

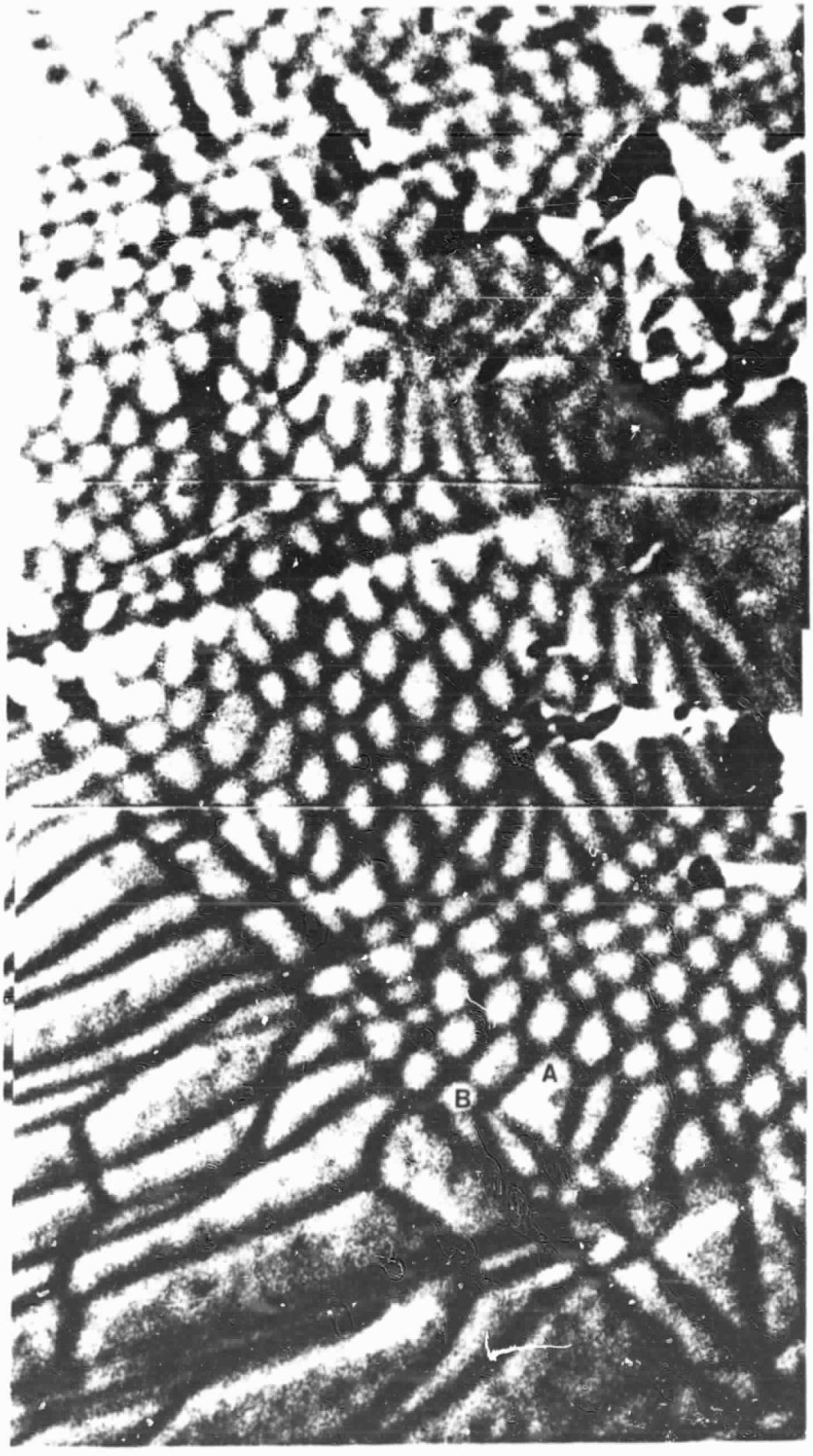

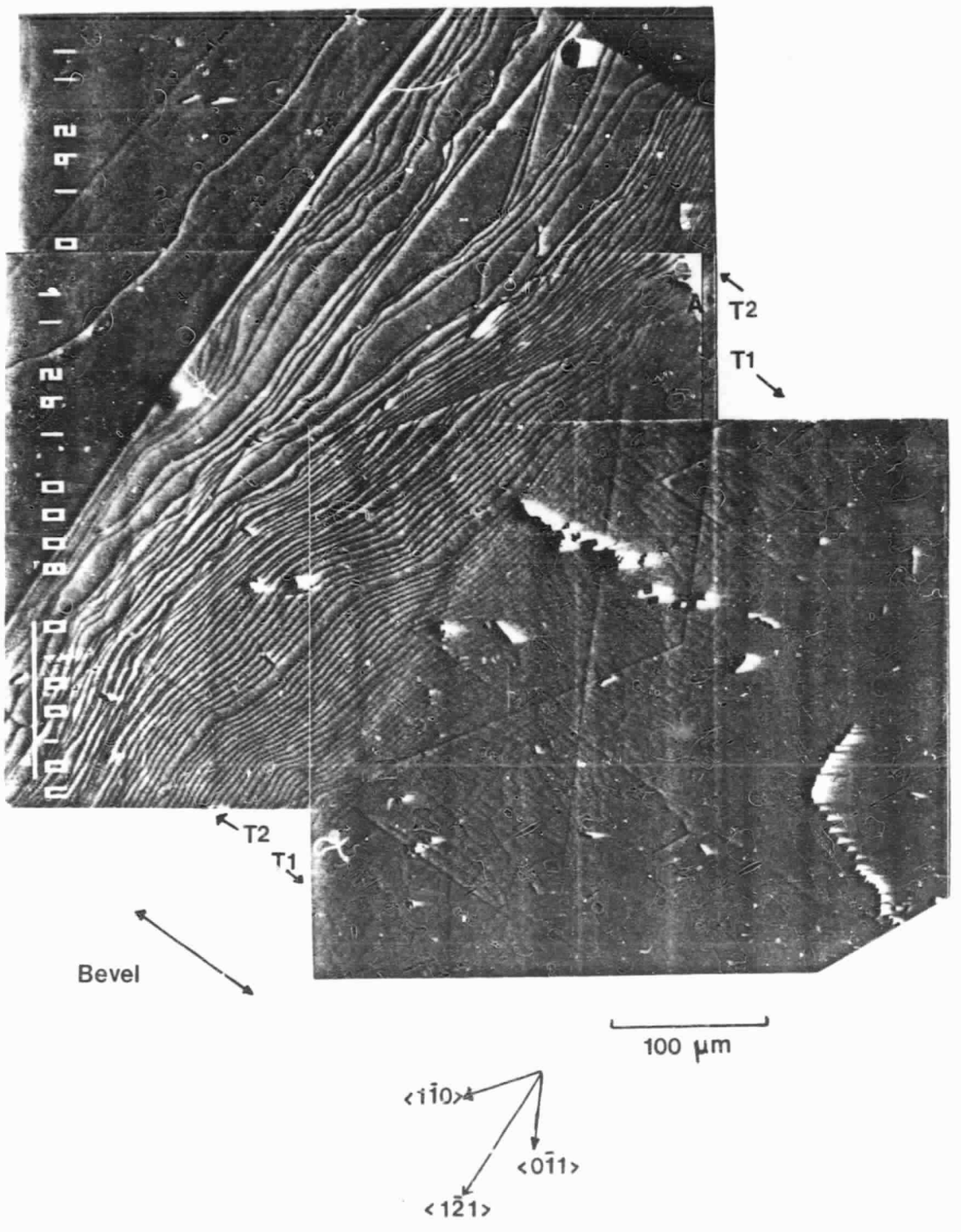

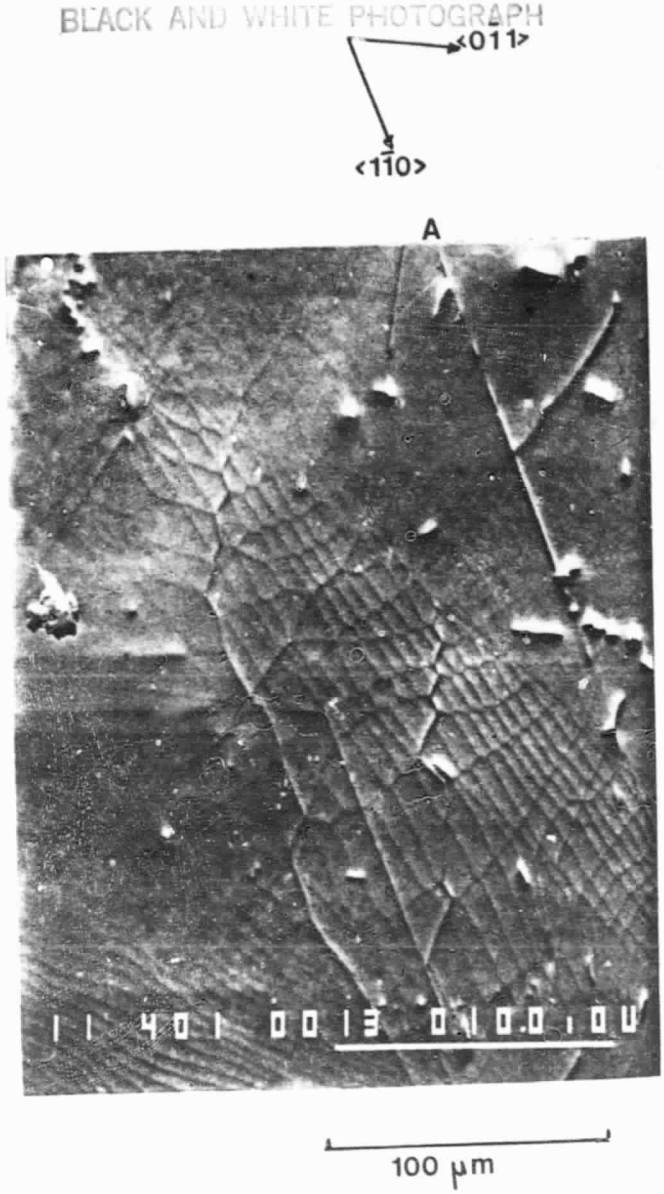

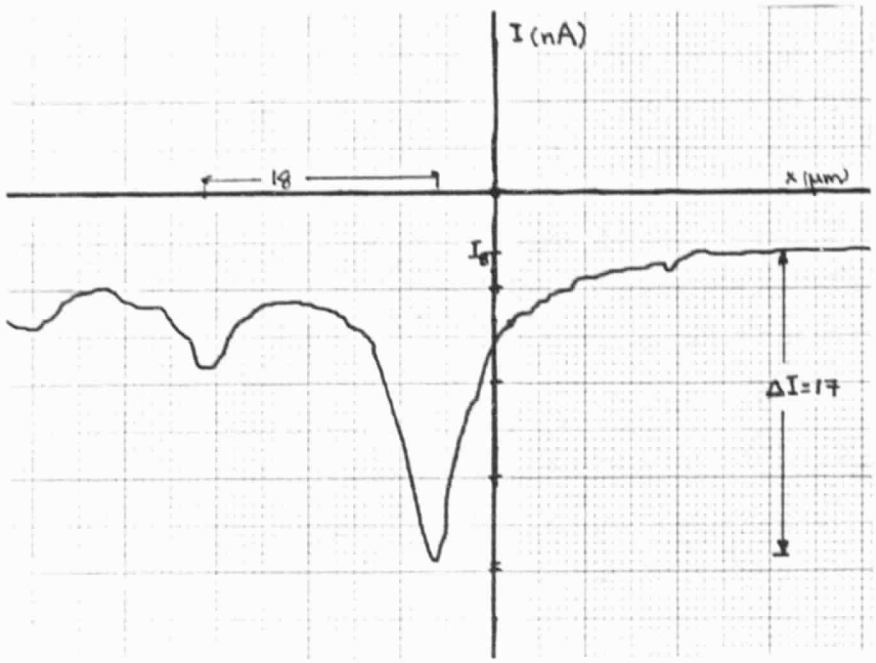

A

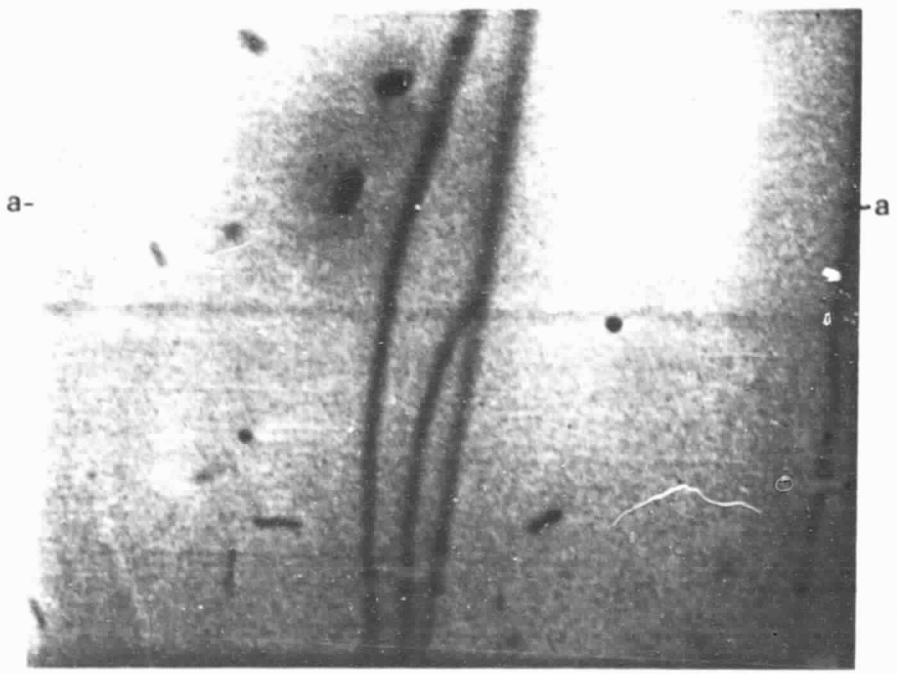

B